Soft Matter

Dynamic Article Links

Cite this: *Soft Matter*, 2011, **7**, 68

www.softmatter.org

PAPER

A functionally graded shape memory polymer†

Andrew M. DiOrio,‡[a] Xiaofan Luo,‡[ab] Kyung Min Lee[c] and Patrick T. Mather*[ab]

Received 8th June 2010, Accepted 27th July 2010
DOI: 10.1039/c0sm00487a

In this article we describe the preparation and characterization of a functionally graded shape memory polymer (SMP) that, unlike conventional SMPs, has a range of transition temperatures that are spatially distributed in a gradient fashion within one single article. This is achieved by post-curing a pre-cured glassy SMP in a linear temperature gradient that imposes different vitrification temperature limits at different positions along the gradient. Utilizing indentation-based surface shape memory coupled with optical measurements of photoelastic response, the capability of this material to respond over a wide range of thermal triggers is examined and correlated with the graded glass transition behavior. The shape recovery response of the gradient SMP under a condition of continuous heating is demonstrated. This new class of SMP offers great potential for such applications as passive temperature sensing and precise control of shape evolution during a thermally triggered shape recovery.

Introduction

Shape memory polymers (SMPs) are a class of "smart" materials that can switch between two shapes on command, from a fixed (temporary) shape to a pre-determined permanent shape upon the application of an external stimulus such as heat.[1–5] This shape memory behavior is generally characterized using programmed, cyclic thermomechanical tests referred to as the shape memory cycle (SMC). In a typical SMC, the SMP is first deformed at an elevated temperature that is higher than its transition temperature, T_{trans} (either T_m or T_g). The deformation is elastic in nature and mainly leads to a reduction in conformational entropy of the constituent network chains, following the rubber elasticity theory.[6] Commonly applied deformation modes include tension, compression, and bending. The deformed SMP is then cooled to a temperature below its T_{trans} while maintaining constant the external strain or stress. During cooling, the material transitions to a more rigid state (semi-crystalline or glassy), which kinetically traps or "freezes" the constituent network chains in this low-entropy state. Macroscopically the material retains, or "fixes," the temporary strain/shape even when external stress is released. Shape recovery is finally triggered by heating the material through T_{trans} under a stress-free (unconstrained)—or even loaded (constrained)—condition. By allowing the network chains (with regained mobility) to relax to their thermodynamically favored, maximal-entropy state, the material changes from the temporary to its permanent shape. Two characteristic ratios, fixing ratio (R_f) and recovery ratio (R_r), characterize the shape memory performance (shape fixing and shape recovery) for comparison among different material systems.[2,5]

SMPs have several intrinsic advantages over the traditionally used shape memory alloys (SMAs) including larger deformation strains, tunable transition temperatures, low density and low manufacturing cost. As a result they have attracted a significant amount of research interest during the past decade. Novel SMPs have been developed with responsiveness to non-heat stimuli such as light,[7] electricity,[8,9] and magnetic field,[10] and with new recovery behavior including two-way shape memory[11,12] and triple-shape memory.[13–17]

The stimuli-responsiveness gives SMPs an ability to sense environmental changes such as an increase of temperature, and respond in a prescribed manner.[18] However, the application of conventional SMPs as temperature sensors is still limited, mainly due to the fact that there is usually only one T_{trans} associated with a given material, as determined by its constituent molecular composition and architecture. In other words, conventional SMPs only respond to a threshold temperature trigger and are unable to respond to temperatures over a broad range.

To overcome this limitation, we applied the concept of functionally graded materials (FGMs)[19–26] to SMPs, the basis of our idea being the control of glass transition temperature of a thermosetting system by the spatially localized ambient temperature during

[a]*Department of Biomedical and Chemical Engineering, Syracuse University, Syracuse, NY, 13244, USA. E-mail: ptmather@syr.edu*
[b]*Syracuse Biomaterials Institute, Syracuse University, Syracuse, NY, 13244, USA*
[c]*Department of Chemical Engineering, Case Western Reserve University, Cleveland, OH, 44106, USA*

† Electronic supplementary information (ESI) available: Scheme S1: the dumbbell geometry used for bulk shape memory characterization, Fig. S1: temperature–distance plots for different temperature gradients generated by varying the heating temperature, Fig. S2: indentation force–depth results for gradient samples 1–10, Fig. S3: loading–unloading curves for NOA63 indented at $T > T_g$, Fig. S4: a continuous movie of Fig. 6, Fig. S5: birefringence (photoelasticity) based demonstrations of gradient recovery, and Table S1: summary of studies on indentation based shape memory. See DOI: 10.1039/c0sm00487a

‡ These authors contributed equally to this work.

photo-crosslinking. The term, FGM, refers to any synthetic material that has spatially dependent compositions, microstructures and associated properties. The FGM concept has engaged a significant amount of research effort since its first introduction in the 1980s, with applications ranging from aerospace to tissue engineering.[27] A variety of fabrication and processing techniques have been developed for polymeric FGMs, including UV polymerization with patterned photo-filters,[19] photodegradation with a gradually removed mask,[20] thermal curing in a temperature gradient,[21] controlled interdiffusion of polymer bilayers,[22] co-extrusion with specially designed gradient distribution and 2-dimensional mixing units,[23] and extrusion followed by laminate molding.[24]

In the present study, we designed and prepared a novel SMP that has a spatially graded glass transition temperature. This is unique among all existing SMPs, to our knowledge, and was technically achieved by post-curing the material (a thiol–ene based photo-crosslinkable glassy thermoset formulation) in a linear temperature gradient, allowing vitrification to occur at different temperatures along the gradient. The resulting material shows a one-dimensional gradient of glass transition temperatures (T_g's) from T_{min} to T_{max}. Therefore the material can respond to a range of temperatures, $T_{min} < T < T_{max}$, yielding a spatially dependent elastic modulus for a given temperature and a spatially dependent shape recovery response upon application of spatially uniform external heating.

To characterize the position-dependent shape memory properties, it is apparent that conventional, bulk characterization methods described above are not ideal since they are based on macroscopic deformations (tension, compression, or bending) that do not have required spatial resolution. Needed are microscopic deformations (with length scales that are smaller than the characteristic distance for T_g to change with the gradient, $\delta = \Delta T_g/(dT_g/dx)$, with ΔT_g being the T_g breadth) that fix and recover "locally" without interfering with each other. For properties of the present case, described below, $\delta \approx 0.5$ mm. Consequently a good candidate for shape memory characterization is indentation,[28] a method that has been applied to SMP research with micro-[29,30] and nano-indentation[31–33] by several authors. For a large variety of synthetic chemistries and compositions utilized among these studies, it was uniformly observed that excellent heat-induced recovery of vitrified indents occurs for all of the SMPs studied. A table summarizing these studies is provided in ESI†. This led us to an expectation that, among glassy SMPs, similar shape memory fixing and recovery for the indentation geometry should be possible. The analytical tools that have been used to monitor and quantify indentation recovery have included either profilometry[30] or atomic force microscopy (AFM).[31–33] While these tools have allowed high spatial resolution for quantification of shape recovery, they are relatively slow and do not provide adequate time resolution of typical recovery events. Inspired by the work of Lu and Shinozaki,[34] we successfully utilized the photoelastic effect, observed using polarized optical microscopy (POM), to monitor and analyze indent recovery. Practically speaking, this can serve as a good readout method for the actual sensing applications.

Overall our functionally graded SMP not only meets the requirements for temperature sensing, but also provides a potential route for precisely controlling the shape recovery profile; for example, directional shape recovery from one end to the other. In what follows, we start by describing the experimental protocols used for preparing and characterizing this functionally graded SMP. Then we present the detailed results and analysis showing the spatially graded shape memory properties. Finally, the gradient shape recovery behavior of our material under continuous heating is demonstrated.

Experimental

Fabrication of temperature gradient hot stage

A custom made temperature gradient hot stage was used to impart T_g gradient to our SMP system, shown in Scheme 1. The stage was designed and fabricated following a technical guide published by NIST.[35] A temperature gradient is produced by heating at one end (*via* a heating unit) and maintaining a constant low temperature (*via* a cooling unit) at the other end. The heating unit consists of a cartridge heater (output power = 300 W, Mcmaster-Carr) and a temperature controller (ETR-9090 from OGDEN Manufacturing Company) with a type T thermocouple. The cooling unit functions by circulating cold water at a constant flow rate using a submersion pump (model 1C-MD-1, March MFG., Inc.). Thermal insulation between the entire apparatus and the laboratory table is provided by two machined Teflon blocks. Besides varying the temperatures of the heating and cooling units, the temperature gradient can be further controlled *via* adjusting the distance between both units by the use of two positioning slots. The actual temperature gradient was verified by measuring the temperatures at different positions using a thermometer (S1-II from Fluke Corporation).

Preparation of functionally graded SMP samples

The SMP used in this study is a commercial UV curable glassy thermoset (Norland Optical Adhesive 63 or NOA63), purchased from Norland Products, Inc. The liquid formulation is polymerized to a solid state *via* thiol–ene step-growth photopolymerization chemistry.[36] Nevertheless, the exact chemical composition of this commercial product is unknown. Uncured NOA63 (a clear, viscous liquid) was first uniformly coated on a glass slide with a controlled thickness of 0.6 mm using a micrometre-based, doctor-blade film applicator (Gardco Microm-II from Paul N. Gardner Company, Inc.). Curing was carried out by exposing NOA63 to 365 nm UV irradiation (Spectroline SB-100P high intensity UV lamp) at room temperature (rt) for 1 h. This resulted in a NOA63 film with a single, uniform T_g of *ca.* 30 °C (measured by DSC). Although dynamic mechanical analysis of this polymer was previously reported to better understand its use in nano-scale microcontact printing,[37] it has not been previously reported as an SMP to the best of our knowledge.

To introduce a T_g gradient, the cured NOA63 film (on a glass slide) was placed on the temperature gradient plate and post-cured under the same UV source for an additional time of 1 h. More details are provided in the next section (Results and discussion), as variations thereof caused systematic changes in the material behavior.

Thermal, mechanical and bulk shape memory characterization

The thermal and mechanical properties of NOA63 were studied using differential scanning calorimetry (DSC) and dynamic

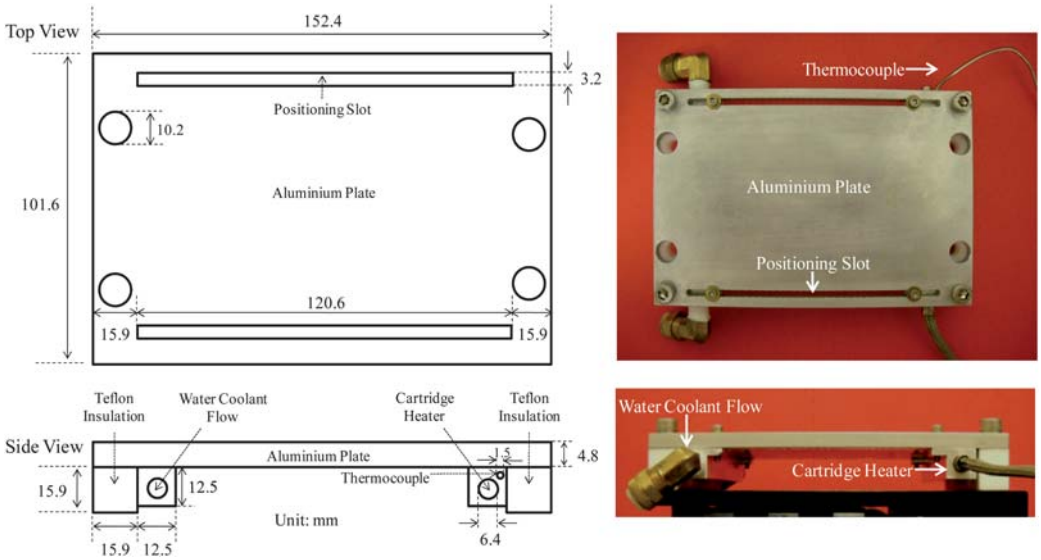

Scheme 1 Technical drawing (left) and photographs (right) of the temperature gradient hot-stage.

mechanical analysis (DMA). For the former, a typical sample of 3–5 mg was encapsulated in a T_{zero} aluminium pan, and examined using a TA Q200 DSC (TA Instruments, Inc.). The temperature was first ramped from 40 °C to 80 °C, then cooled back to −60 °C, and finally ramped to 80 °C while collecting the heat flow data. Both heating and cooling rates were 10 °C min^{-1}. The T_g was determined as the mid-point of the step transition in heat flow during the 2nd heating. For DMA, a rectangular film (7.24 mm × 3.56 mm × 0.19 mm) was loaded under tension on a TA Q800 dynamic mechanical analyzer (TA Instruments, Inc.). An oscillatory deformation with an amplitude of 15 μm, a frequency of 1 Hz, and a "force track" (ratio of static to dynamic force) of 115% was applied while ramping the temperature from −90 °C to 100 °C at 3 °C min^{-1}.

The bulk shape memory of cured NOA63 was characterized using a well established four-step thermomechanical cycling method, referred to as the one-way shape memory (1WSM) cycle.[1,2,5,12,18] Since this involved large-strain tensile deformation, a dumbbell geometry guided by ASTM D638 (ESI†) was used, successfully avoiding sample failure at the grips that often plagues thin film SMP testing. Film thicknesses of 0.16 mm were utilized. Each sample, loaded under tension, was: (1) stretched to a tensile strain of 31% by ramping the force to 0.5 N (corresponding to a stress of 2 MPa) at a constant rate of 0.05 N min^{-1} at 70 °C ($T > T_g$), (2) cooled back to 20 °C ($T < T_g$) followed by an isothermal hold for 10 min, (3) unloaded by ramping the force to 0.01 N at the same rate of 0.05 N min^{-1} to witness strain fixing and (4) heated to 70 °C to allow strain recovery under no constraint. The same procedure was then repeated for two more times to assess the deterioration in shape memory performance, if any, as a result of thermomechanical cycling. To further analyze the shape memory results, fixing ratio (R_f) and recovery ratio (R_r) were calculated according to:[2,5]

$$R_f(N) = \frac{\varepsilon_u(N)}{\varepsilon_m(N)} \times 100\% \quad (1)$$

$$R_r(N) = \frac{\varepsilon_u(N) - \varepsilon_p(N)}{\varepsilon_u(N) - \varepsilon_p(N-1)} \times 100\% \quad (2)$$

here ε_m, ε_u, ε_p and N stand for the strain before unloading, the strain after unloading, the permanent strain after heating (strain that is not recovered) and the cycle number, respectively. For cycle 1 ($N = 1$), $\varepsilon_p(0)$ is taken as the initial strain at the onset of the experiment.

Micro-indentation of functionally graded NOA63

A post-cured NOA63 was cut evenly into 10 separate pieces along the length (T_g gradient) direction. Samples were spaced by 2 mm or a T_g difference of about 0.5 °C. Each piece was then indented on a rheometer (ARG2, TA Instruments) using the gap-control feature of the instrument and normal force transducer, along with a custom-assembled indenter setup (Scheme 2). The indenter tip was made from a Pfanstiehl diamond stylus (352-D7 from KAB Electro Acoustics) with a well-defined conical geometry (Scheme 2, tip radius ≈ 25 μm), bonded to the center of a 25 mm disposable aluminium plate. The sample, placed on the bottom plate, was indented at 80 °C ($T > T_g$; temperature controlled by a thermal chamber, known as the environmental testing chamber or ETC on the above mentioned rheometer) by bringing the indenter tip (or top plate) down at a constant speed

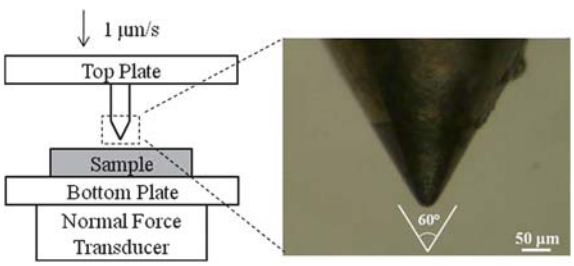

Scheme 2 The micro-indentation setup.

of 1 μm s^{-1} until a maximum normal force of 0.4 N was reached. Then, the sample was quickly cooled (10 °C min^{-1}) to 25 °C ($T < T_g$) while holding the normal force constant. The normal force was finally released by raising the indenter (top plate) away from the sample at 1 μm s^{-1}.

Indent recovery and image analysis method

As mentioned in the introduction, the strain field induced by indentation could be visualized semi-quantitatively as birefringence based on the photoelastic effect. When heated, the birefringence would disappear in sync with the stress field and (for SMPs with good recovery) the strain field. At the molecular level this is due to the oriented polymer chains relaxing back to their thermodynamically favored random coil confirmations. Experimentally this was monitored by an Olympus BX51 optical microscope with crossed polarizer and analyzer, coupled with an Instec HCS402 hot-stage. Digital micrographs (24 bit color) were taken every 30 s by a QICAM FAST-1394 CCD camera while heating the sample from 25 °C to 65 °C at a linear heating rate of 2 °C min^{-1}.

The digital images were then converted to 8 bit grayscale using Photoshop CS2. The histogram of each image was analyzed to obtain the average pixel intensity ($\bar{I}$) by dividing the overall greyscale intensity (integration of the histogram) by the total number of pixels, using a constant region of interest (ROI) area of 1160 μm × 870 μm which covers the entire birefringence zone (as shown in Fig. 4). The $\bar{I}$ of the last image (the one taken at 65 °C) was used as the background noise (I_B) to calculate the normalized intensity (I_N):

$$I_N = \frac{\bar{I} - I_B}{I_0 - I_B} \quad (3)$$

where I_0 is the $\bar{I}$ of the first (25 °C) image. The normalized intensity, I_N, was then plotted as a function of temperature for each sample, quantifying indentation recovery temperature and breadth with spatial resolution achieved by the small indenter size.

Demonstration of gradient shape recovery

To further demonstrate the gradient shape recovery behavior, a functionally graded NOA63 film was prepared, with dimensions of 7.5 cm (length) × 2.3 cm (width) × 0.28 mm (thickness). A series of cuts spaced along the T_g-gradient (length) direction were cut through the film thickness and along the film width direction using a razor blade. The cuts started from the edge and ended around the center of the film width (1.1–1.2 cm long), and were 5 mm apart from the adjacent ones. The sample was then heated at 80 °C, folded along its "center line" (parallel to the film length), and cooled to room temperature to fix the deformation. A Pelletier plate (an accessory of the ARG2 rheometer) was used to uniformly heat the material and trigger its recovery. For this purpose, the deformed sample was placed on the Pelletier system, with the "virgin" (uncut) half-surface actually touching the Pelletier plate. A glass slide was put on top of the virgin half-surface to enhance thermal contact. With this configuration, the recovery of each "finger" (the area between two adjacent cuts) can occur without much mechanical constraint, or under a relatively stress-free condition. In other words, the recovery of each finger is not affected by the recovery of the adjacent fingers, and is solely determined by its localized T_g (the average T_g of that finger). The temperature was linearly ramped from 25 °C to 60 °C at 2 °C min^{-1} with images taken every minute (or every 2 °C) using a digital camera. A compilation of these images in the form of a video is provided in ESI†.

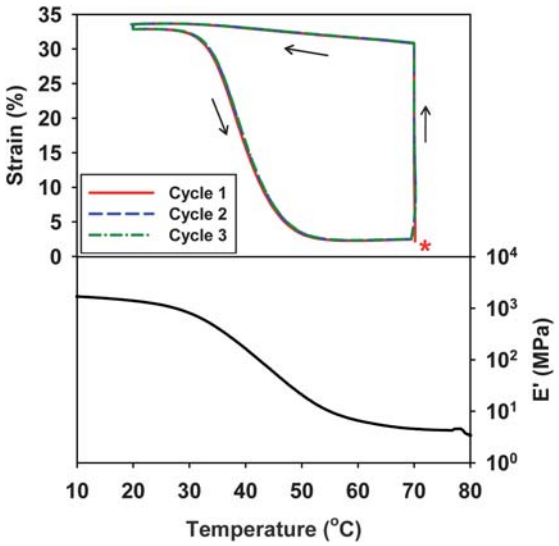

Fig. 1 The bulk 1WSM cycles (top: the asterisk indicates experimental onset) and temperature dependent DMA result (bottom) of cured NOA63 (no post-cure).

Results and discussion

Cured NOA63 is a transparent, glassy solid that has excellent shape memory properties as shown in Fig. 1. In this case the material was cured under UV for 1 h at rt (the actual temperature was ~5 °C higher due to the heating effect of UV irradiation) without any further post-cure and shows a uniform T_g of 29.7 °C (determined from the onset of E' drop). It is observed from the 1WSM cycles (Fig. 1, top) that, a large percentage of strain was fixed after unloading at 20 °C, corresponding to an R_f of 98.4% (averaged over three cycles; the same below for R_r). The fixed strain recovered almost completely ($R_r = 99.7\%$) in a relatively small temperature range during heating. Furthermore, the shape memory performance showed no deterioration up to three cycles, in that all the curves follow almost exactly with each other. This indicates good thermal stability of cured NOA63.

The T_g of cured NOA63 was found to increase in response to post-photocure at higher temperatures. This can be interpreted based on reaction kinetics. When NOA63 is being photo-cured, the T_g increases with conversion until it reaches the environmental temperature, T_e. Vitrification (transition from rubbery to glassy state) takes place which significantly limits the reaction rate due to reduced chain mobility/diffusion. When the environmental temperature is raised to T_e' ($T_e' > T_g$); however, the polymer chains re-enter the rubbery state and the residual reaction resumes, until the material T_g reaches T_e' or T_u, whichever is lower. Here, T_u is the ultimate T_g the material can potentially

reach (determined by network chain composition) at 100% conversion. Therefore the material T_g can be controlled precisely by controlling T_e', as long as T_e' is lower than T_u. In this sense, our method is not expected to work for semicrystalline networks (Class II SMPs[1]), which are thermally or photocured well above the vitrification point. It is also worth noting that in the specific case of NOA63, we found that heat and UV irradiation are both required to raise the T_g. Heating by itself does not change the T_g tangibly. This is evident from the 1WSM cycles in Fig. 1; if heating was to change the T_g, the recovery transitions of the second and third cycles would have shifted to higher temperature, rather than staying almost constant. This is understandable since NOA63 polymerizes *via* a free radical mechanism, and UV is the only means to generate free radicals (by the decomposition of remaining UV initiators) in the system.

Based on the above discussions, post-curing NOA63 on a temperature gradient would therefore introduce a T_g gradient on the material. For this purpose, a temperature gradient hot-stage was fabricated. By controlling the heating (*via* a cartridge heater) at one end and cooling (*via* cold water circulation) at the other end, a series of linear temperature gradients can be easily produced (Fig. S1†). For the post-curing of NOA63, we utilized a linear temperature gradient from 36 to 65 °C along the sample length (70 mm, filled circles in Fig. 2). The actual temperatures at the glass slide surface (temperature NOA63 was actually experiencing) were also measured and a large "damping" effect was observed, which reduced the temperature gradient from 36–65 °C to 33–51 °C (hollow circles in Fig. 2). The DSC-measured sample T_g's closely matched the glass slide temperatures and spanned from 30 to 48 °C, or a gradient of 2.7 °C cm^{-1}. This also proved that the reaction was indeed vitrification-limited.

To study the functionally graded shape memory properties, another post-cure was carried out and the resulting film was evenly cut into 10 samples along the gradient direction, as described in the Experimental section. The samples are referred to as sample 1 to 10, where the sample numbers increase with decreasing T_g, as will be shown. Each sample was indented to

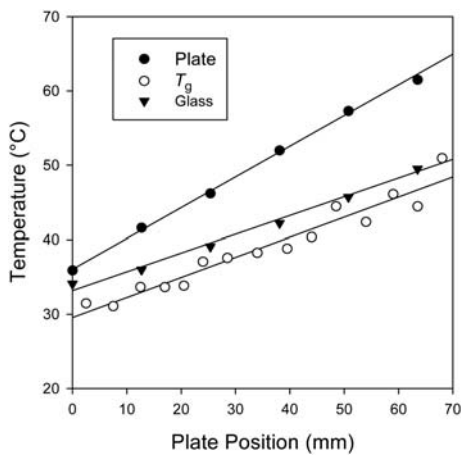

Fig. 2 The temperature *vs.* position plots for the temperature gradient hot-stage (●), the glass slide (○) and the T_g's (measured by DSC) on the final NOA63 film (▼). The temperature of the "heater" end was set to be 120 °C (see Scheme 1) while ice-water circulation was maintained at the "cooler" end.

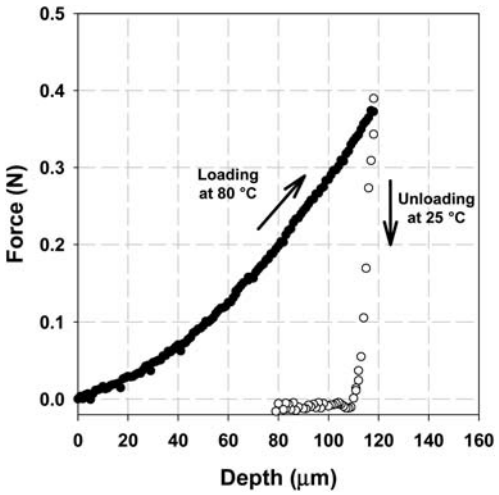

Fig. 3 Force *vs.* depth curves showing the loading step at 80 °C (●) and the unloading step at 25 °C (○) for sample 9 (see text as well as Fig. 5).

a maximum normal force of 0.4 N at 80 °C. This resulted in a penetration distance, or an indent depth of *ca.* 120 μm as shown in Fig. 3 (for clarity only the sample 9 is shown, please see ESI† for the other samples). Since the material existed in its rubbery state (80 °C ≫ T_g), the deformation was primarily elastic. This is supported by the experimental observation that the loading and unloading yielded very similar force-depth curves with minimal hysteresis (ESI†). Microscopically, this deformation led to conformational changes (orientation) of the polymer chain segments. Similar to the fixing of a macroscopic deformation (Fig. 1), the indented sample was cooled to 25 °C while holding the force constant. During cooling, the polymer went through its T_g and as a result, the conformational changes of chain segments were "frozen" due to a significant decrease of mobility and the indent was "fixed". The latter can be seen from Fig. 3 in that the depth decreased only slightly from 118 to 110 μm after unloading at 25 °C. In other words 93.2% of the deformation was fixed.

The indent was then visualized under POM, and a classical "four-leaf" birefringent pattern could be observed (Fig. 4), which reflects the strain field surrounding the indent.[34] When heated, both the intensity and the total area of the pattern decreased

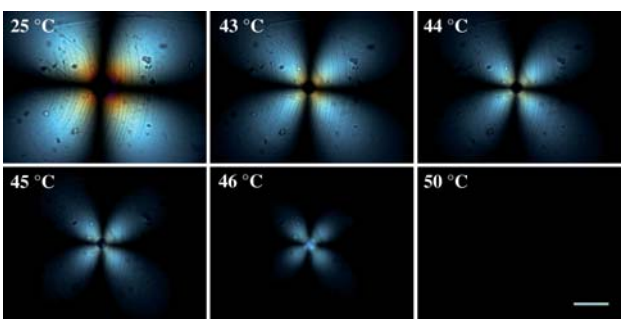

Fig. 4 Polarized optical microscopy (POM) images showing the recovery of an indent during heating. Shown here is the sample 9 (see text as well as Fig. 5) which has a DSC-measured T_g of 43 °C. The scale bar represents 200 μm.

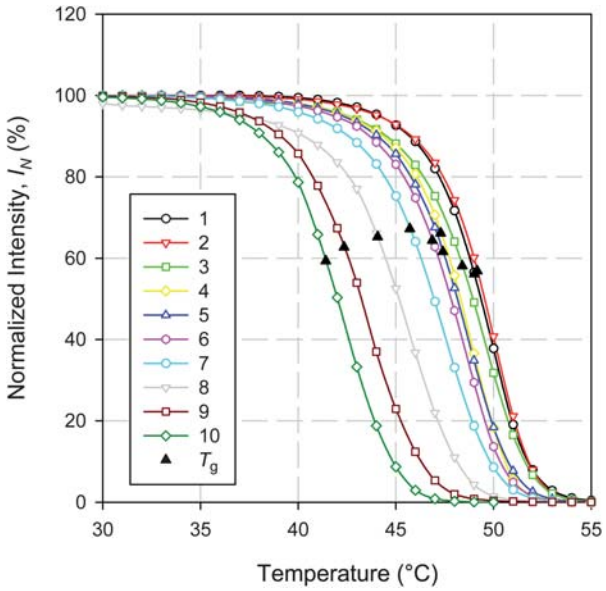

Fig. 5 The indent recoveries, shown as the normalized birefringence intensity (%) *vs.* temperature (°C) plots, for samples 1–10 (see text for details). The filled triangles stand for DSC-measured T_g's for all the samples.

gradually with temperature. The image became eventually dark, indicating the fact that the strain had fully recovered, and all the chain segments had relaxed back to their thermodynamically favored random coil conformations.

The indent recovery was further studied by image analysis, in which the normalized intensity of each image was plotted as a function of temperature for samples 1 to 10 (Fig. 5). The DSC-measured T_g's for each sample are also indicated in the graph (filled triangles in Fig. 5). For all the samples, a sigmoidal-like recovery profile similar to the recovery of macroscopic deformation (Fig. 1) was seen. It is clear that the indent recovered at higher temperatures with increased T_g's, and the DSC-measured T_g always corresponded to the temperature with a normalized intensity of *ca.* 60% (or 40% of the intensity recovery). We further demonstrated this gradient recovery behavior in a macroscopically visible manner. The experimental details were described in the Experimental section and the result is shown in Fig. 6. The material has an increasing T_g from left to right, as the arrow in Fig. 6 indicates. For this sample, the T_g varied from *ca.* 30 °C on the left-hand side to 50 °C on the right hand side, while the gradient was "sampled" by slicing along the gradient direction to give 15 "fingers" along the bottom edge, each marked on its terminus with a black dot. In this configuration, each finger featured T_g variation < 1.5 °C. Uniform heating was provided by the Pelletier plate on which the sample was placed. The plate temperature was linearly ramped from 25 °C to 60 °C at 2 °C min^{-1}. As anticipated, the recovery initiated at the left end (where the T_g was lowest) and propagated to the right with increasing temperature. A movie compilation of a full collection of images during heating and two more demonstrations using a birefringence-detecting optical setup are provided in ESI†.

Finally, we consider the potential application of functionally graded SMPs for temperature sensing. A material with a known one-dimensional T_g gradient (such as the graded NOA63 presented in this article) can be fixed thermomechanically with localized deformations, such as a series of evenly spaced indents along the gradient direction. Heating such a specimen to a temperature T within its T_g range (between T_{min} and T_{max}) would result in the recovery of indents located between T_{min} and T but not T and T_{max}. Therefore examining the recovery profile by some means would allow the precise determination of T. Considering d to be the spatial resolution of indentation recovery detection, the temperature sensing resolution, ΔT, is then given by either $(d \times dT_g/dx)$ if $d \geq \delta$ (δ being the characteristic distance defined in Introduction), or $(\delta \times dT_g/dx)$ if $d < \delta$. In the former case, the sensing resolution can be enhanced (lowering ΔT) by reducing the temperature gradient dT_g/dx. This can, in turn, be controlled by the external temperature gradient, as shown in Fig. 2. In the latter case, since $\delta = \Delta T_g/(dT_g/dx)$ (ΔT_g being the

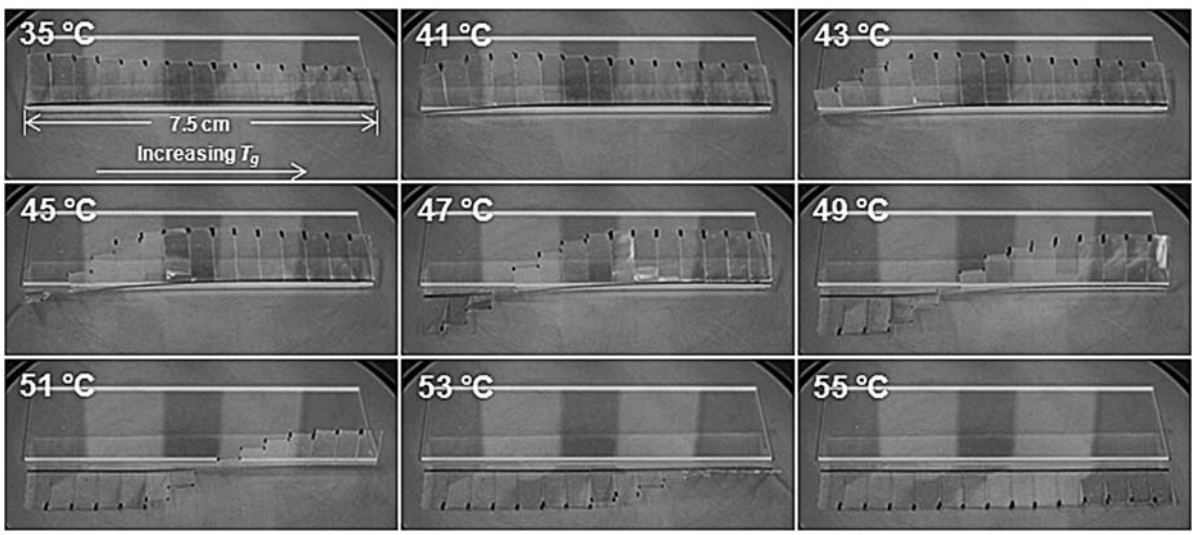

Fig. 6 Visual demonstration of the gradient recovery behavior of a functionally graded NOA63. The arrow in the first (35 °C) image indicates the direction of T_g gradient. More experimental details can be found in the Experimental section.

T_g breadth), the above expression becomes $\Delta T = \Delta T_g$. This indicates that the sensing resolution is material-limiting when $d < \delta$. Therefore the only way to enhance the resolution would be to reduce ΔT_g.

Due to the simplicity of the presented material and fabrication method, we envision the production of low-cost "temperature labels" that could be utilized to measure temperatures in areas that are not accessible by conventional methods or not amenable to continuous monitoring, to indirectly indicate sterilization completion, or for incorporation into product packaging (for shipping industry or food storage) to indicate the maximum temperature of product exposure.

Conclusions

In conclusion, a functionally graded SMP encompassing a range of T_g's distributed in a gradient fashion has been successfully fabricated by post-curing the material in a linear temperature gradient. Utilizing indentation-based surface shape memory, the gradient recovery properties of the material were explored and its ability to respond to a broad temperature range was demonstrated. Further, a macroscopic manifestation of the functionally graded shape memory phenomenon was demonstrated. Owing to its simplicity and optical characteristics, this new class of SMPs offers great potential for material-based temperature sensors as well as applications where controlled shape evolution during recovery is desired.

Acknowledgements

The authors gratefully acknowledge discussions with Pushkar Varde and Tarun Saxena of Prof. Julie Hasenwinkel's research group at Syracuse University concerning the stylus adopted for indentation testing. Ellen Benn is acknowledged for help in editing the article. PTM is grateful for funding from AFOSR (FA9550-09-1-0195) and NSF (DMR-0907578), which partially supported this research.

Notes and references

1 C. Liu, H. Qin and P. T. Mather, *J. Mater. Chem.*, 2007, **17**, 1543–1558.
2 P. T. Mather, X. F. Luo and I. A. Rousseau, *Annu. Rev. Mater. Res.*, 2009, **39**, 445–471.
3 A. Lendlein and S. Kelch, *Angew. Chem., Int. Ed.*, 2002, **41**, 2034–2057.
4 D. Ratna and J. Karger-Kocsis, *J. Mater. Sci.*, 2008, **43**, 254–269.
5 I. A. Rousseau, *Polym. Eng. Sci.*, 2008, **48**, 2075–2089.
6 L. R. G. Treloar, *The Physics of Rubber Elasticity*, Clarendon Press, Oxford, 3rd edn, 1975.
7 A. Lendlein, H. Y. Jiang, O. Junger and R. Langer, *Nature*, 2005, **434**, 879–882.
8 Y. J. Liu, H. B. Lv, X. Lan, J. S. Leng and S. Y. Du, *Compos. Sci. Technol.*, 2009, **69**, 2064.
9 X. F. Luo and P. T. Mather, *Soft Matter*, 2010, **6**, 2146–2149.
10 R. Mohr, K. Kratz, T. Weigel, M. Lucka-Gabor, M. Moneke and A. Lendlein, *Proc. Natl. Acad. Sci. U. S. A.*, 2006, **103**, 3540–3545.
11 H. H. Qin and P. T. Mather, *Macromolecules*, 2009, **42**, 273–280.
12 T. Chung, A. Rorno-Uribe and P. T. Mather, *Macromolecules*, 2008, **41**, 184–192.
13 I. Bellin, S. Kelch, R. Langer and A. Lendlein, *Proc. Natl. Acad. Sci. U. S. A.*, 2006, **103**, 18043–18047.
14 M. Bell and A. Lendlein, *J. Mater. Chem.*, 2010, **20**, 3335–3345.
15 T. Xie, X. C. Xiao and Y. T. Cheng, *Macromol. Rapid Commun.*, 2009, **30**, 1823–1827.
16 T. Pretsch, *Smart Mater. Struct.*, 2010, **19**, 015006.
17 X. F. Luo and P. T. Mather, *Adv. Funct. Mater.*, DOI: 10.1002/adfm.201000052.
18 J. Kunzelman, T. Chung, P. T. Mather and C. Weder, *J. Mater. Chem.*, 2008, **18**, 1082–1086.
19 J. Y. Wong, A. Velasco, P. Rajagopalan and Q. Pham, *Langmuir*, 2003, **19**, 1908–1913.
20 X. F. Yao, D. L. Liu and H. Y. Yeh, *J. Appl. Polym. Sci.*, 2007, **106**, 3253–3258.
21 P. Z. Zhao, X. Y. Hua, Y. S. Wang, J. H. Zhu and Q. Z. Wen, *Mater. Sci. Eng., A*, 2007, **457**, 231–235.
22 B. Hexig, H. Alata, N. Asakawa and Y. Inoue, *J. Polym. Sci., Part B: Polym. Phys.*, 2005, **43**, 368–377.
23 Y. B. Zhu, N. Y. Ning, Y. Sun, Q. Zhang and Q. Fu, *Macromol. Mater. Eng.*, 2006, **291**, 1388–1396.
24 B. Y. Wen, G. Wu and J. Yu, *Polymer*, 2004, **45**, 3359–3365.
25 F. M. Gallant, H. A. Bruck and A. K. Kota, *J. Compos. Mater.*, 2004, **38**, 1873–1893.
26 K. K. U. Stellbrink, G. Hausser and R. Steegmuller, *J. Thermoplast. Compos. Mater.*, 1999, **12**, 188–200.
27 B. Kieback, A. Neubrand and H. Riedel, *Mater. Sci. Eng., A*, 2003, **362**, 81–105.
28 W. C. Oliver and G. M. Pharr, *J. Mater. Res.*, 1992, **7**, 1564–1583.
29 K. Gall, P. Kreiner, D. Turner and M. Hulse, *J. Microelectromech. Syst.*, 2004, **13**, 472–483.
30 B. Xu, W. M. Huang, Y. T. Pei, Z. G. Chen, A. Kraft, R. Reuben, J. T. M. De Hosson and Y. Q. Fu, *Eur. Polym. J.*, 2009, **45**, 1904–1911.
31 E. Wornyo, K. Gall, F. Z. Yang and W. King, *Polymer*, 2007, **48**, 3213–3225.
32 F. Yang, E. Wornyo, K. Gall and W. P. King, *Nanotechnology*, 2007, **18**, 285302.
33 F. Z. Yang, E. Wornyo, K. Gall and W. P. King, *Scanning*, 2008, **30**, 197–202.
34 Y. C. Lu and D. M. Shinozaki, *J. Eng. Mater. Technol.*, 2008, **130**, 7.
35 *Temperature Gradient Stage: Specifications and Operation Guidelines*, NIST Combinatorial Methods Center, 2005, accessed at http://polymers.msel.nist.gov/combi/Instrumentation/06%20Temperature%20Gradient%20Stage.pdf.
36 C. E. Hoyle, T. Y. Lee and T. Roper, *J. Polym. Sci., Part A: Polym. Chem.*, 2004, **42**, 5301–5338.
37 J. Park, Y. S. Kim and P. T. Hammond, *Nano Lett.*, 2005, **5**, 1347–1350.

